Harmonic assessment of variable-speed wind turbines considering a converter control malfunction

R. Melício[1], V.M.F. Mendes[2], and J.P.S. Catalão[1]

[1] Department of Electromechanical Engineering, University of Beira Interior, R. Fonte do Lameiro, 6201-001 Covilha, Portugal

catalao@ubi.pt

[2] Department of Electrical Engineering and Automation, Instituto Superior de Engenharia de Lisboa, R. Conselheiro Emídio Navarro, 1950-062 Lisbon, Portugal

vfmendes@isel.pt

Abstract: This paper is on variable-speed wind turbines with permanent magnet synchronous generator. Three different drive train mass models and three different topologies for the power-electronic converters are considered. The three different topologies considered are respectively a matrix, a two-level and a multilevel converter. A novel control strategy, based on fractional-order controllers, is proposed for the wind turbines. The influence of a converter control malfunction on the harmonic current emissions is studied. The performance of disturbance attenuation and system robustness is ascertained. Simulation results are presented, and conclusions are duly drawn.

Key words: Wind power; power converters; harmonic assessment; fractional-order control

List of symbols

u	wind speed value with disturbance
u_0	average wind speed
A_k	magnitude of the eigenswing k
ω_k	eigenfrequency of the eigenswing k
P_{tt}	mechanical power of the turbine
ρ	air density
R	radius of the area covered by the blades
c_p	power coefficient
ω_t	rotor angular speed at the wind turbine
θ	pitch angle of the rotor blades
λ	tip speed ratio
P_t	mechanical power of the wind turbine disturbed by the mechanical eigenswings
m	order of the harmonic of a eigenswing
g_{km}	distribution of the m-order harmonic in the eigenswing k
a_{km}	normalized magnitude of g_{km}
h_k	modulation of eigenswing k
φ_{km}	phase of the m-order harmonic in the eigenswing k
J	moment of inertia for blades, hub and generator of the one-mass model
J_t	moment of inertia for blades and hub of the two-mass model
T_t	mechanical torque
T_{dt}	resistant torque in the wind turbine bearing of the two-mass model

T_{at} resistant torque in the hub and blades of the two-mass model

T_{ts} torsional stiffness torque of the two-mass model

ω_g rotor angular speed at the generator

J_g moment of inertia for the rotor of the generator

T_{dg} resistant torque in the generator bearing of the two-mass model

T_{ag} resistant torque due to the viscosity of the airflow in the generator of the two-mass model

T_g electrical torque

J_b moment of inertia of the flexible blades section of the three-mass model

J_h moment of inertia of the hub and the rigid blades section of the three-mass model

T_{db} resistant torque of the flexible blades of the three-mass model

T_{bs} torsional flexible blades stiffness torque of the three-mass model

T_{dh} resistant torque of the rigid blades and the hub of the three-mass model

T_{ss} torsional shaft stiffness torque of the three-mass model

T_{dg} resistant torque of the generator of the three-mass model

i_f equivalent rotor current

M mutual inductance

p number of pairs of poles

i_d, i_q stator currents

L_d, L_q stator inductances

R_d, R_q stator resistances

u_d, u_q stator voltages

1 Introduction

The study of harmonic current emissions associated with renewable energy technologies is essential in order to analyse their effect on the electrical grids where they are connected [1, 2]. Among the renewable energy technologies, wind turbine technology is now the world's fastest growing energy source. Wind turbines achieve an excellent technical availability of about 98% on average, although they have to face a high number of malfunctions [3].

The quick wind power augmentation presents a global style although Europe continues to dominate the global market [4]. In Portugal, the wind power goal foreseen for 2010 has been recently established by the government as 5100 MW [5]. Hence, Portugal has one of the most ambitious goals in terms of wind power, and in 2006 was the second country in Europe with the highest wind power growth.

As the penetration level of wind power in power systems increases, the overall performance of the electrical grid will increasingly be affected by the characteristics of wind turbines. One of the major concerns related to the high penetration level of the wind turbines is the impact on power system stability [6]. Also, network operators have to ensure that consumer power quality is not compromised. Hence, the total harmonic distortion (THD) should be kept as low as possible, improving the quality of the energy injected into the electrical grid [7].

Power-electronic converters have been developed for integrating wind power with the electrical grid. The use of power-electronic converters allows for variable-speed operation of the wind turbine and enhanced power extraction [8]. In a recent overview of different wind generator systems [9], it has been shown that variable speed concepts with power electronics will continue to dominate and be very promising technologies for large wind farms.

In a variable-speed wind turbine with full-power converter, the wind turbine is directly connected to the generator and the generator is completely decoupled from the electrical grid.

Accurate modelling and control of wind turbines have high priority in the research activities all over the world [10]. At the moment, substantial documentation exists on modelling and control issues for the doubly fed induction generator (DFIG) wind turbine. But this is not the case for wind turbines with permanent magnet synchronous generator (PMSG) and full-power converter. Hence, a PMSG is considered in this paper.

Previous papers were mainly focused on the transient stability of variable-speed wind turbines at external grid faults [11–13]. Grid code specifications in European countries require that wind turbines must be able to ride though grid disturbances that bring voltages down to very low levels [14]. Accordingly, great effort has been made to develop variable-speed wind turbines capable of supporting voltage/frequency and remain connected to the system during external grid faults [15, 16], but little attention has been given to the possibility of internal abnormal operating conditions, such as a converter control malfunction, using different drive train mass models.

Hence, this paper focuses on the harmonic assessment of wind turbines with PMSG and full-power converters, considering: (i) three different drive train mass models, respectively, one, two and three mass models; (ii) three different topologies for power-electronic converters, respectively matrix, two-level and multilevel converters; (iii) a novel fractional-order control strategy; (iv) a converter control malfunction.

2 Modelling

2.1 Wind speed

The wind speed usually varies considerably and has a stochastic character. The wind speed variation can be modelled as a sum of harmonics with frequency range 0.1–10 Hz [17]:

$$u = u_0 \left[1 + \sum_k A_k \sin(\omega_k \, t) \right] \tag{1}$$

Hence, the physical wind turbine model is subjected to the disturbance given by the wind speed variation model [18].

2.2 Wind turbine

The mechanical power of the turbine is given by:

$$P_{tt} = \frac{1}{2} \rho \pi R^5 \frac{\omega_t^3}{\lambda^3} c_p \tag{2}$$

The computation of the power coefficient requires the use of blade element theory and the knowledge of blade geometry. In this paper, the numerical approximation developed in [19] is followed, where the power coefficient is given by:

$$c_p = 0.73 \left(\frac{151}{\lambda_i} - 0.58\theta - 0.002\theta^{2.14} - 13.2 \right) e^{-\frac{18.4}{\lambda_i}} \tag{3}$$

$$\lambda_i = \frac{1}{\dfrac{1}{(\lambda - 0.02\theta)} - \dfrac{0.003}{(\theta^3 + 1)}} \tag{4}$$

The global maximum for the power coefficient is at null pitch angle and it is equal to:

$$c_{p\max}(\lambda_{opt}(0), 0) = 0.4412 \tag{5}$$

corresponding to an optimal tip speed ratio at null pitch angle equal to:

$$\lambda_{opt}(0) = 7.057 \tag{6}$$

The conversion of wind energy into mechanical energy over the rotor of a wind turbine is influenced by various forces acting on the blades and on the tower of the wind turbine (e.g. centrifugal, gravity and varying aerodynamic forces acting on blades, gyroscopic forces acting on the tower), introducing mechanical effects influencing the energy conversion. Those mechanical effects have been modelled by eigenswings mainly due to the following phenomena: asymmetry in the turbine, vortex tower interaction, and eigenswing in the blades. The mechanical power over the rotor of the wind turbine has been modelled, using the mechanical eigenswings [18], as a set of harmonic terms multiplied by the power associated with the energy capture from the wind by the blades, given by:

$$P_t = P_{tt} \left[1 + \sum_{k=1}^{3} A_k \left(\sum_{m=1}^{2} a_{km} \, g_{km}(t) \right) h_k(t) \right] \tag{7}$$

$$g_{km} = \sin\left(\int_0^t m\,\omega_k(t')\,dt' + \varphi_{km}\right) \tag{8}$$

The values used on (1), (7) and (8) for the calculation of P_t are given in Table 1 [18].

Table 1: Mechanical eigenswings excited in the wind turbine

k	Source	A_k	ω_k [rad/s]	h_k	m	a_{km}	φ_{km}
1	Asymmetry	0.01	ω_t	1	1	4/5	0
					2	1/5	$\pi/2$
2	Vortex tower interaction	0.08	$3\ \omega_t$	1	1	1/2	0
					2	1/2	$\pi/2$
3	Blades	0.15	$9\ \pi$	$1/2\ (g_{11}+g_{21})$	1	1	0

2.3 Drive train models

In a one-mass drive train model, all components are lumped together and modelled as a single rotating mass. The equation for the one-mass model is based on the second law of Newton, deriving the state equation for the rotor angular speed at the wind turbine, given by:

$$\frac{d\omega_t}{dt} = \frac{1}{J}\left(T_t - T_g\right) \tag{9}$$

A comparative study of wind turbine generator system using different drive train models [20] has shown that the two-mass model may be more suitable for transient stability analysis.

The equations for the two-mass model are based on the torsional version of the second law of Newton, deriving the state equation for the rotor angular speed at the wind turbine and for the rotor angular speed at the generator, respectively given by:

$$\frac{d\omega_t}{dt} = \frac{1}{J_t}\left(T_t - T_{dt} - T_{at} - T_{ts}\right) \tag{10}$$

$$\frac{d\omega_g}{dt} = \frac{1}{J_g}\left(T_{ts} - T_{dg} - T_{ag} - T_g\right) \tag{11}$$

With the increase in size of the wind turbines, one question arises whether long flexible blades have an important impact on the transient stability analysis of wind power systems during a fault [21]. To determine the dynamic properties of the blade, finite element techniques may be used but this approach cannot easily be implemented in power systems analysis programs. Hence, to avoid the use of the finite element approach it is necessary to simplify the rotor dynamics as much as possible. One way to achieve this is represented in Fig. 1, where the blade analysis is represented as a simple torsional system. Since the blade bending occurs at a significant distance from the joint between the blade and the hub, the blade can be split in two parts, OA and AB. The blade sections OA1, OA2 and OA3 are the rigid blade sections and have the moment of inertia J_h; the blade sections A1B1, A2B2 and A3B3 are the flexible blade sections and have the moment of inertia J_b [22]. The configuration of the three-mass model is shown in Fig. 2.

The equations for the three-mass model are also based on the torsional version of the second law of Newton. They are respectively given by:

$$\frac{d\omega_t}{dt} = \frac{1}{J_b}\left(T_t - T_{db} - T_{bs}\right) \tag{12}$$

$$\frac{d\omega_h}{dt} = \frac{1}{J_h}\left(T_{bs} - T_{dh} - T_{ss}\right) \tag{13}$$

$$\frac{d\omega_g}{dt} = \frac{1}{J_g}\left(T_{ss} - T_{dg} - T_g\right) \tag{14}$$

2.4 Generator

The state equations for modelling the PMSG stator currents, using motor machine convention, are given by:

$$\frac{di_d}{dt} = \frac{1}{L_d}\left[u_d + p\,\omega_g\,L_q\,i_q - R_d\,i_d\right] \tag{15}$$

$$\frac{di_q}{dt} = \frac{1}{L_q}\left[u_q - p\,\omega_g\left(L_d\,i_d + M\,i_f\right) - R_q\,i_q\right] \tag{16}$$

In order to avoid demagnetization of permanent magnet in the PMSG, a null stator current $i_d = 0$ is imposed [23]. The electrical power is given by:

$$P_g = [u_d \quad u_q \quad u_f][i_d \quad i_q \quad i_f]^T \tag{17}$$

2.5 Matrix converter

The matrix converter is an AC-AC converter, with nine bidirectional commanded insulated gate bipolar transistors (IGBTs) S_{ij}. It is connected between a first order filter and a second order filter. The first order filter is connected to a PMSG, while the second order filter is connected to an electrical grid. A switching strategy can be chosen so that the output voltages have nearly sinusoidal waveforms at the desired frequency, magnitude and phase angle, and the input currents are nearly sinusoidal at the desired displacement power factor [24]. The phase currents injected into the electrical grid are modelled by the state equation given by:

$$\frac{di_{fj}}{dt} = \frac{1}{L_n}(u_{fj} - R_n\, i_{fj} - u_j) \qquad j = \{4,5,6\} \tag{18}$$

The configuration of the simulated wind power system with matrix converter is shown in Fig. 3.

The IGBTs commands S_{ij} in function of the on and off states are given by:

$$S_{ij} = \begin{cases} 1, \text{ (on)} \\ 0, \text{(off)} \end{cases} \qquad i, j \in \{1, 2, 3\} \tag{19}$$

subject to the constraints given by:

$$\sum_{j=1}^{3} S_{ij} = 1 \qquad i \in \{1, 2, 3\} \tag{20}$$

$$\sum_{i=1}^{3} S_{ij} = 1 \qquad j \in \{1, 2, 3\} \tag{21}$$

The vector of output phase voltages in function of the vector of input phase voltages [25] is given by:

$$\begin{bmatrix} v_A \\ v_B \\ v_C \end{bmatrix} = \begin{bmatrix} S_{11} & S_{12} & S_{13} \\ S_{21} & S_{22} & S_{23} \\ S_{31} & S_{32} & S_{33} \end{bmatrix} \begin{bmatrix} v_a \\ v_b \\ v_c \end{bmatrix} = [S] \begin{bmatrix} v_a \\ v_b \\ v_c \end{bmatrix} \tag{22}$$

The vector of input phase currents in function of the vector of output phase currents [25] is given by:

$$[i_a \quad i_b \quad i_c]^T = [S]^T \, [i_A \quad i_B \quad i_C]^T \tag{23}$$

2.6 Two-level converter

The two-level converter is an AC/DC/AC converter, with six unidirectional commanded IGBTs used as a rectifier, and with the same number of unidirectional commanded IGBTs used as an inverter. Each IGBT is indicated by its switching state S_{ij}. The index i with $i \in \{1,2\}$ identifies the IGBT. A group of two IGBTs linked to the same phase constitute a leg j of the converter. The index j with $j \in \{1,2,3\}$ identifies a leg for the rectifier and $j \in \{4,5,6\}$ identifies the inverter one. The rectifier is connected between the PMSG and a capacitor bank. The inverter is connected between this capacitor bank and a second order filter, which in turn is connected to an electrical grid [26, 27]. The phase currents injected into the electrical grid are modelled by the state equation (18).

The configuration of the wind power system with two-level converter is shown in Fig. 4.

A switching variable γ_j of each leg j is used to identify the state of the IGBT i in the leg j of the converter. The switching variable of each leg j [28] is given by:

$$\gamma_j = \begin{cases} 1, \ (S_{1j} = 1 \ \text{and} \ S_{2j} = 0) \\ 0, \ (S_{1j} = 0 \ \text{and} \ S_{2j} = 1) \end{cases} \qquad j \in \{1, \ldots, 6\} \tag{24}$$

Hence, each switching variable depends on the conducting and blocking states of the IGBTs. The voltage v_{dc} is modelled by the state equation given by:

$$\frac{dv_{dc}}{dt} = \frac{1}{C}\left(\sum_{j=1}^{3} \gamma_j i_j - \sum_{j=4}^{6} \gamma_j i_j \right) \tag{25}$$

2.7 Multilevel converter

The multilevel converter is an AC/DC/AC converter, with twelve unidirectional commanded IGBTs S_{ij} used as a rectifier, and with the same number of unidirectional commanded IGBTs used as an inverter. A group of four IGBTs linked to the same phase constitute a leg j of the converter. The rectifier is connected between the PMSG and a capacitor bank. The inverter is connected between this capacitor bank and a second order filter, which in turn is connected to an electrical grid [26, 27]. The phase currents injected into the electrical grid are modelled by the state equation (18).

The configuration of the wind power system with multilevel converter is shown in Fig. 5.

The switching variable γ_j of each leg j is a function of the states S_{ij} of the converter. The index i with $i \in \{1,2,3,4\}$ identifies the IGBT. The index j with $j \in \{1,2,3\}$ identifies the leg for the rectifier and $j \in \{4,5,6\}$ identifies the inverter one. The switching variable of each leg j are subject to the constraints [29] given by:

$$\gamma_j = \begin{cases} 1, & (S_{1j} \text{ and } S_{2j}) = 1 \quad \text{and} \quad (S_{3j} \text{ or } S_{4j}) = 0 \\ 0, & (S_{2j} \text{ and } S_{3j}) = 1 \quad \text{and} \quad (S_{1j} \text{ or } S_{4j}) = 0 \\ -1, & (S_{3j} \text{ and } S_{4j}) = 1 \quad \text{and} \quad (S_{1j} \text{ or } S_{2j}) = 0 \end{cases} \qquad j \in \{1, \ldots ,6\} \tag{26}$$

A switching variable Φ_{1j} is associated with the two upper IGBTs in each leg j (S_{1j} and S_{2j}), and also a switching variable Φ_{2j} is associated with the two lower IGBTs (S_{3j} and S_{4j}), respectively given by:

$$\Phi_{1j} = \frac{\gamma_j(1+\gamma_j)}{2} \quad ; \quad \Phi_{2j} = \frac{\gamma_j(1-\gamma_j)}{2} \qquad j \in \{1, \ldots ,6\} \tag{27}$$

Hence, each switching variable depends only on the conducting and blocking states of the IGBTs. The voltage v_{dc} is the sum of the voltages v_{C1} and v_{C2} in the capacitor banks C_1 and C_2, modelled by the state equation given by:

$$\frac{dv_{dc}}{dt} = \frac{1}{C_1}\left(\sum_{j=1}^{3}\Phi_{1j}i_j - \sum_{j=4}^{6}\Phi_{1j}i_j\right) + \frac{1}{C_2}\left(\sum_{j=1}^{3}\Phi_{2j}i_j - \sum_{j=4}^{6}\Phi_{2j}i_j\right) \tag{28}$$

3 Control strategy

3.1 Fractional-order controller

A novel control strategy based on fractional-order PI^{μ} controllers is proposed for the variable-speed operation of wind turbines with PMSG and full-power converters. Fractional calculus theory is a generalization of ordinary differentiation and integration to arbitrary (non-integer) order [30]. Fractional-order calculus used in mathematical models of the systems can improve the design, properties and controlling abilities in dynamical systems [31, 32]. A fractional order controller has a dynamical behaviour described by a fractional differential integral equation with derivatives and integrals having at least one not integer order. The design of a fractional order controller has the advantage of entailing more criterion than the conventional PI controller, augmenting the freedom for achieving an enhanced behaviour.

The fractional-order differentiator can be denoted by a general operator ${}_aD_t^{\mu}$ [33], given by:

$$
{}_aD_t^{\mu} = \begin{cases} \dfrac{d^{\mu}}{dt^{\mu}}, & \Re(\mu) > 0 \\ 1, & \Re(\mu) = 0 \\ \int_a^t (d\tau)^{-\mu}, & \Re(\mu) < 0 \end{cases} \tag{29}
$$

where μ is the order of derivative or integral, $\Re(\mu)$ is the real part of the μ. The mathematical definition of fractional derivatives and integrals has been the subject of several descriptions. The most frequently encountered one is called Riemann–Liouville definition, in which the fractional-order integral is given by:

$$
{}_aD_t^{-\mu} f(t) = \frac{1}{\Gamma(\mu)} \int_a^t (t-\tau)^{\mu-1} f(\tau)\, d\tau \tag{30}
$$

while the definition of fractional-order derivatives is given by:

$$
{}_aD_t^{\mu} f(t) = \frac{1}{\Gamma(n-\mu)} \frac{d^n}{dt^n} \left[\int_a^t \frac{f(\tau)}{(t-\tau)^{\mu-n+1}} d\tau \right] \tag{31}
$$

where:

$$\Gamma(x) \equiv \int_0^\infty y^{x-1} e^{-y} dy \tag{32}$$

is the Euler's Gamma function, a and t are the limits of the operation, and μ is the number identifying the fractional order. In this paper, μ is assumed as a real number that satisfies the restrictions $0 < \mu \leq 1$. Also, it is assumed that $a = 0$. The following convention is used: ${}_0D_t^{-\mu} \equiv D_t^{-\mu}$.

The other approach is Grünwald–Letnikov definition of fractional-order integral given by:

$${}_aD_t^{-\mu} f(t) = \lim_{h \to 0} h^{\mu} \sum_{r=0}^{\frac{t-a}{h}} \frac{\Gamma(\mu + r)}{r! \Gamma(\mu)} f(t - rh) \tag{33}$$

while the definition of fractional-order derivatives given by:

$${}_aD_t^{\mu} f(t) = \lim_{h \to 0} h^{-\mu} \sum_{r=0}^{\frac{t-a}{h}} (-1)^r \frac{\Gamma(\mu + 1)}{r! \Gamma(\mu - r + 1)} f(t - rh) \tag{34}$$

where the binomial coefficients $(r > 0)$ are given by:

$$\binom{\mu}{0} = 1, \quad \binom{\mu}{r} = \frac{\mu(\mu - 1) \ldots (\mu - r + 1)}{r!} \tag{35}$$

An important property revealed by (33) is that while integer-order operators imply finite series, the fractional-order counterparts are defined by infinite series [32, 33]. This means that integer operators are local operators in opposition with the fractional operators that have, implicitly, a memory of all past events.

The differential equation of the fractional-order PI^{μ} controller, $0 < \mu < 1$, in time domain, is given by:

$$u(t) = K_p e(t) + K_i D_t^{-\mu} e(t) \tag{36}$$

where K_p is a proportional constant and K_i is an integration constant. Taking $\mu = 1$ in (36), a conventional PI controller is obtained.

Hence, using Laplace transforms the transfer function of the fractional-order PI^{μ} and proportional integral PI controllers are respectively given by:

$$G(s) = K_p + K_i\, s^{-\mu} \tag{37}$$

$$G(s) = K_p + K_i\, s^{-1} \tag{38}$$

3.2 Converters control

Power converters are variable structure systems, because of the on/off switching of their IGBTs. Sliding mode control presents special interest for systems with variable structure, such as switching power converters, guaranteeing the choice of the most appropriate space vectors. The aim is to let the system slide along a predefined sliding surface by changing the system structure. The sliding mode control presents attractive features such as robustness to parametric uncertainties of the wind turbine and the generator as well as to electrical grid disturbances [25, 34].

The power semiconductors present physical limitations that have to be considered during design phase and during simulation study. Particularly, they cannot switch at infinite frequency. Also, for a finite value of the switching frequency, an error $e_{\alpha\beta}$ will exist between the reference value and the control value. In order to guarantee that the system slides along the sliding surface $S(e_{\alpha\beta},t)$, it has been proven that it is necessary to ensure that the state trajectory near the surfaces verifies the stability conditions [25] given by:

$$S(e_{\alpha\beta},t)\,\frac{dS(e_{\alpha\beta},t)}{dt} < 0 \tag{39}$$

in practice a small error $\varepsilon > 0$ for $S(e_{\alpha\beta},t)$ is allowed, due to power semiconductors switching only at finite frequency. Consequently, a switching strategy has to be considered given by:

$$-\varepsilon < S(e_{\alpha\beta},t) < +\varepsilon \tag{40}$$

A practical implementation of the switching strategy considered in (40) could be accomplished by using hysteresis comparators.

The outputs of the hysteresis comparators are the integer variables $\sigma_{\alpha\beta} = (\sigma_\alpha, \sigma_\beta)$ [25]. For the two-level converter, σ_α and σ_β assume values in the set Ω given by:

$$\Omega \in \{-1, 0, 1\} \tag{41}$$

The appropriate vectors selection in order to ensure stability for the two-level converter is shown in Table 2.

Table 2: Output voltage vectors selection for the two-level converter

$\sigma_\beta \backslash \sigma_\alpha$	-1	0	1
-1	4	4;5	5
0	6	0;7	1
1	2	3;2	3

For the multilevel converter, σ_α and σ_β assume values in the set Ω given by:

$$\Omega \in \{-2, -1, 0, 1, 2\} \tag{42}$$

In this control strategy, only when $v_{C1} \neq v_{C2}$ a new vector is selected. The appropriate vectors selection in order to ensure stability for the multilevel converter is shown in Table 3, for $v_{C1} > v_{C2}$, and in Table 4, for $v_{C1} < v_{C2}$.

Table 3: Output voltage vectors selection for the multilevel converter, for $v_{C1} > v_{C2}$

$\sigma_\beta \backslash \sigma_\alpha$	-2	-1	0	1	2
-2	25	25	12	7	7
-1	24	13	13;6	6	8
0	19	18	1;14;27	5	9
1	20	17	17;2	2	4
2	21	21	16	3	3

Table 4: Output voltage vectors selection for the multilevel converter, for $v_{C1} < v_{C2}$

$\sigma_\beta \backslash \sigma_\alpha$	-2	-1	0	1	2
-2	25	25	12	7	7
-1	24	26	26;11	11	8
0	19	23	1;14;27	10	9
1	20	22	22;15	15	4
2	21	21	16	3	3

4. Harmonic assessment

The harmonic behaviour computed by the Discrete Fourier Transform (DFT) is given by:

$$X(k) = \sum_{n=0}^{N-1} e^{-j2\pi k n/N} x(n) \quad \text{for} \quad k = 0,..., N-1 \tag{43}$$

where $x(n)$ is the input signal and $X(k)$ is the amplitude and phase of the different sinusoidal components of $x(n)$.

The harmonic behaviour computed by the THD is given by:

$$\text{THD}\ (\%) = 100 \frac{\sqrt{\sum_{H=2} X_H^2}}{X_F} \tag{44}$$

where X_H is the root mean square (RMS) value of the individual harmonic components of the signal, and X_F is the RMS value of the fundamental component.

The IEC 61400-21 standard [35], the standard applying power quality requirements for grid-connected wind turbines, recommends limiting the flicker emissions [36]. However, this paper focuses only on the harmonic emissions. Standards such as IEEE-519 [37] impose limits for different order harmonics and the THD. The limit is 5% for THD. Hence, IEEE-519 standard is used in this paper as a guideline for comparison purposes.

5 Simulation results

The wind power system considered has a rated electrical power of 900 kW, and the time horizon considered in the simulation is 4 s. Table 5 summarizes the wind power system data.

Table 5: Wind power system data

Turbine moment of inertia	2500×10^3 kgm²
Turbine rotor diameter	49 m
Tip speed	17.64-81.04 m/s
Rotor speed	6.9-31.6 rpm
Generator rated power	900 kW
Generator moment of inertia	100×10^3 kgm²

The mathematical models for the wind power system with the matrix, two-level and multilevel converters were implemented in Matlab/Simulink. In this paper, $\mu = 0.7$ is initially considered. The switching frequency used in the simulation results is 5 kHz.

The average wind speed considered is a ramp wind speed starting at 10 m/s and stabilizing after 1.5 s at 20 m/s.

$$u(t) = u_0 \left[1 + \sum_k A_k \sin(\omega_k \, t) \right] \qquad 0 \le t \le 4 \tag{45}$$

Fig. 6 shows the wind speed profile, while Fig. 7 shows the tip speed of the blades.

On possible way to simulate a malfunction was to consider a random choice on the voltage vectors for the power converters. Hence, a converter control malfunction is assumed to occur between 2 s and 2.02 s modelled by a random selection of the voltage vectors for the matrix converter and for the inverter of the two-level and the multilevel converters, respectively.

5.1 Ideal sinusoidal voltage waveforms on the network

The simulation results for a network modelled as a three-phase active symmetrical circuit in series, with 850 V at 50 Hz, were carried out.

Fig. 8 shows what happens to the vectors selection on the converter before and after the converter control malfunction, for the matrix converter and a three-mass model. Fig. 9 shows the output RMS current for the matrix converter and a three-mass model.

Fig. 10 shows what happens to the vectors selection on the inverter before and after the converter control malfunction, for the two-level converter and a three-mass model. Fig. 11 shows the voltage v_{dc} for the two-level converter and a three-mass model. Fig. 12 shows the output RMS current for the two-level converter and a three-mass model.

Fig. 13 shows what happens to the vectors selection on the inverter before and after the converter control malfunction, for the multilevel converter and a three-mass model. Fig. 14

shows the voltage v_{dc} for the multilevel converter and a three-mass model. Fig. 15 shows the output RMS current for the multilevel converter and a three-mass model.

The harmonic behaviour of the current injected into the electrical grid, computed by the DFT, is shown in Figs. 16, 17 and 18 for the matrix, two-level and multilevel converters, respectively, and a three-mass model.

Table 6 presents the values of the fundamental component of the current injected into the electrical grid, computed by the DFT, for the three power converter topologies and the three drive train mass models.

Table 6: Fundamental component of the current injected into the electrical grid

Wind power system	Fundamental (%) with three-mass model	Fundamental (%) with two-mass model	Fundamental (%) with one-mass model
Matrix converter	81.90	82.52	82.82
Two-level converter	92.89	93.29	93.69
Multilevel converter	93.01	93.41	93.70

The THD of the current injected into the electrical grid is shown in Figs. 19, 20 and 21 for the matrix, two-level and multilevel converters, respectively, and a three-mass model.

Table 7 presents the average THD of the current injected into the electrical grid for the three power converter topologies and the three drive train mass models.

Table 7: Average THD of the current injected into the electrical grid

Wind power system	THD (%) with three-mass model	THD (%) with two-mass model	THD (%) with one-mass model
Matrix converter	2.80	2.40	2.08
Two-level converter	0.75	0.56	0.52
Multilevel converter	0.61	0.57	0.51

The harmonics are related to the power electronic conversion system and their control. The presence of the energy-storage elements, in comparison with the matrix converter, and the increasing number of voltage levels, in comparison with the two-level converter, allows the wind power system with the multilevel converter to achieve the best performance. Nevertheless, for all power converter topologies, the average THD of the current injected into the electrical grid is lower than the 5% limit imposed by the IEEE-519 standard.

The drive train model (one, two or three mass-blocks) may imply less or more accurate THD results. On the one hand, the one-mass model provides a less realistic approach; therefore, the THD results may be underestimated, as shown in Table 7. On the other hand, the three-mass model provides a more realistic approach; therefore, more accurate THD results are attainable. The three-mass model may be more appropriate for the precise harmonic assessment of variable-speed wind turbines.

Table 8 summarizes an overall comparison between the conventional PI controller ($\mu = 1$) and fractional-order $PI^{0.5}$ and $PI^{0.7}$ controllers, for the three-mass model, concerning the average THD of the current injected into the electrical grid. As can been seen, the best results are achieved by considering $\mu = 0.7$.

Table 8: Average THD of the current injected into the electrical grid

Wind power system	THD (%) considering PI controller	THD (%) considering $PI^{0.5}$ controller	THD (%) considering $PI^{0.7}$ controller
Matrix converter	3.32	2.93	2.80
Two-level converter	0.94	0.81	0.75
Multilevel converter	0.76	0.64	0.61

5.2 Non-ideal sinusoidal voltage waveforms on the network

The simulation results for a network modelled as a three-phase active symmetrical circuit in series, with 850 V at 50 Hz and 5% of third harmonic component, were carried out.

Table 9 presents the values of the fundamental and third harmonic components of the current injected into the electrical grid, computed by the DFT, for the three power converter topologies and a three-mass model.

Table 9: Fundamental and third harmonic components of the current injected into the electrical grid

Wind power system	Fundamental (%)	3^{rd} harmonic (%)
Matrix converter	72.45	6.97
Two-level converter	85.92	5.99
Multilevel converter	87.77	5.66

Table 10 presents the average THD of the current injected into the electrical grid for the three power converter topologies and a three-mass model.

Table 10: Average THD of the current injected into the electrical grid

Wind power system	THD (%)
Matrix converter	7.12
Two-level converter	3.22
Multilevel converter	2.63

The THD of the current injected into the electrical grid is lower than the 5% limit imposed by IEEE-519 standard for the two-level and multilevel converters, but is higher for the matrix converter. Hence, it has been shown that non-ideal sinusoidal voltage waveforms on the network affect the current THD from the converters.

6 Conclusions

The increased wind power penetration leads to new technical challenges, transient stability and power quality. This paper focuses on the harmonic assessment of wind turbines with PMSG and full-power converters, considering: (i) three different drive train mass models, respectively, one, two and three mass models; (ii) three different topologies for power-electronic converters, respectively matrix, two-level and multilevel converters; (iii) a novel fractional-order control strategy; (iv) a converter control malfunction. The results have shown that the three-mass model may be more appropriate for the precise harmonic assessment of variable-speed wind turbines. Also, the results have shown that the proposed fractional-order controller for the variable-speed operation of wind turbines can effectively decrease the total harmonic distortion.

7 References

1 Simmons, A.D., and Infield, D.G.: 'Current waveform quality from grid-connected photovoltaic inverters and its dependence on operating conditions', *Prog. Photovoltaics*, 2000, **8**, (4), pp. 411–420

2 Tentzrakis, S.T., and Papathanassiou, S.A.: 'An investigation of the harmonic emissions of wind turbines', *IEEE Trans. Energy Convers.*, 2007, **22**, (1), pp. 150–158

3 Hahn, B., Durstewitz, M., and Rohrig, K.: 'Reliability of wind turbines', Renewable Energies Knowledge, 2006, http://www.renknow.net

4 Chen, Z., Hu, Y., and Blaabjerg, F.: 'Stability improvement of induction generator-based wind turbine systems', *IET Renew. Power Gener.*, 2007, **1**, (1), pp. 81–93

5 Estanqueiro, A., Castro, R., Flores, P., Ricardo, J., Pinto, M., Rodrigues, R., and Peças Lopes, J.: 'How to prepare a power system for 15% wind energy penetration: the Portuguese case study', *Wind Energy*, 2008, **11**, (1), pp. 75–84

6 Ullah, N.R., and Thiringer, T.: 'Variable speed wind turbines for power system stability enhancement', *IEEE Trans. Energy Convers.*, 2007, **22**, (1), pp. 52–60

7 Carrasco, J.M., Franquelo, L.G., Bialasiewicz, J.T., Galvan, E., Guisado, R.C.P., Prats, A.M., Leon, J.I., and Moreno-Alfonso, N.: 'Power-electronic systems for the grid integration of renewable energy sources: A survey', *IEEE Trans. Ind. Electron.*, 2006, **53**, (4), pp. 1002–1016

8 Baroudi, J.A., Dinavahi, V., and Knight, A.M.: 'A review of power converter topologies for wind generators', *Renew. Energy*, 2007, **32**, (14), pp. 2369–2385

9 Li, H., and Chen, Z.: 'Overview of different wind generator systems and their comparisons', *IET Renew. Power Gener.*, 2008, **2**, (2), pp. 123–138

10 Hansen, A.D., and Michalke, G: 'Modelling and control of variable-speed multi-pole permanent magnet synchronous generator wind turbine', *Wind Energy*, 2008, **11**, (5), pp. 537–554

11 Conroy, J.F., and Watson, R.: 'Low-voltage ride-through of a full converter wind turbine with permanent magnet generator', *IET Renew. Power Gener.*, 2007, **1**, (3), pp. 182–189

12 Jauch, C.: 'Transient and dynamic control of a variable speed wind turbine with synchronous generator', *Wind Energy*, 2007, **10**, (3), pp. 247–269

13 Kasem, A.H., El-Saadany, E.F., El-Tamaly, H.H., and Wahab, M.A.A.: 'An improved fault ride-through strategy for doubly fed induction generator-based wind turbines', *IET Renew. Power Gener.*, 2008, **2**, (4), pp. 201–214

14 Conroy, J., and Watson, R.: 'Aggregate modelling of wind farms containing full-converter wind turbine generators with permanent magnet synchronous machines: transient stability studies', *IET Renew. Power Gener.*, 2009, **3**, (1), pp. 39–52

15 Ramtharan, G., Ekanayake, J.B., and Jenkins, N.: 'Frequency support from doubly fed induction generator wind turbines', *IET Renew. Power Gener.*, 2007, **1**, (1), pp. 3–9

16 Kanellos, F.D., and Hatziargyriou, N.D.: ‘Control of variable speed wind turbines equipped with synchronous or doubly fed induction generators supplying islanded power systems’, *IET Renew. Power Gener.*, 2009, **3**, (1), pp. 96–108

17 Xing, Z.X., Zheng, Q.L., Yao, X.J., and Jing, Y.J.: ‘Integration of large doubly-fed wind power generator system into grid’, Proc. 8th Int. Conf. Electrical Machines and Systems, Nanjing, China, Sep. 2005, pp. 1000–1004

18 Akhmatov, V., Knudsen, H., and Nielsen, A.H.: ‘Advanced simulation of windmills in the electric power supply’, *Int. J. Electr. Power Energy Syst.*, 2000, **22**, (6), pp. 421–434

19 Slootweg, J.G., de Haan, S.W.H., Polinder, H., and Kling, W.L.: ‘General model for representing variable speed wind turbines in power system dynamics simulations’, *IEEE Trans. Power Syst.*, 2003, **18**, (1), pp. 144–151

20 Muyeen, S.M., Hasan Ali, Md., Takahashi, R., Murata, T., Tamura, J., Tomaki, Y., Sakahara, A., and Sasano, E.: ‘Comparative study on transient stability analysis of wind turbine generator system using different drive train models’, *IET Renew. Power Gener.*, 2007, **1**, (2), pp. 131–141

21 Li, H., and Chen, Z.: ‘Transient stability analysis of wind turbines with induction generators considering blades and shaft flexibility’, Proc. 33rd Annual Conference of the IEEE-Industrial-Electronics-Society, Taiwan, Nov. 2007, pp. 1604–1609

22 Ramtharan, G., Jenkins, N., Anaya-Lara, O., Bossanyi, E.: ‘Influence of rotor structural dynamics representations on the electrical transient performance of FSIG and DFIG wind turbines’, *Wind Energy*, 2007, **10**, (4), pp. 293–301

23 Senjyu, T., Tamaki, S., Urasaki, N., and Uezato, K.: ‘Wind velocity and position sensorless operation for PMSG wind generator’, Proc. 5th Int. Conf. Power Electronics and Drive Systems, Singapore, Nov. 2003, pp. 787–792

24 Barakati, S.M., Aplevich, J.D., and Kazerani, M.: ‘Controller design for a wind turbine system including a matrix converter’, Proc. 2007 IEEE Power Engineering Society General Meeting, Tampa, Florida, Jun. 2007, pp. 779–786

25 Pinto, S., and Silva, J.: ‘Sliding mode direct control of matrix converters’, *IET Electr. Power Appl.*, 2007, **1**, (3), pp. 439–448

26 Melício, R., Mendes, V.M.F., and Catalão, J.P.S.: ‘Two-level and multilevel converters for wind energy systems: a comparative study’, Proc. 13th Int. Power Electronics and Motion Control Conf., Poznań, Poland, Sep. 2008, pp. 1682–1687

27 Melício, R., Mendes, V.M.F., and Catalão, J.P.S.: ‘Evaluating power quality in wind power generation systems with two-level and multi-level converters’, Proc. 6th Mediterranean Conf. and Exhibition on Power Generation, Transmission and Distribution, Thessaloniki, Greece, Nov. 2008

28 Silva, J.F., and Pinto, S.F.: ‘Control methods for switching power converters’, in Rashid, M.H. (Ed.): ‘Power Electronics Handbook’ (Academic Press, 2007), pp. 935–998

29 Barros, J.D., and Silva, J.F.: ‘Optimal predictive control of three-phase NPC multilevel converter for power quality applications’, *IEEE Trans. Ind. Electron.*, 2008, **55**, (10), pp. 3670–3681

30 Podlubny, I.: ‘Fractional-order systems and PI-lambda-D-mu-controllers’, *IEEE Trans. Autom. Control*, 1999, **44**, (1), pp. 208–214

31 Biswas, A., Das, S., Abraham, A., and Dasgupta, S.: ‘Design of fractional-order (PID mu)-D-lambda controllers with an improved differential evolution’, *Eng. Appl. Artif. Intell.*, 2009, **22**, (2), pp. 343–350

32 Cao, J.Y., and Cao, B.G.: ‘Design of fractional order controllers based on particle swarm optimization’, Proc. 1st IEEE Conference on Industrial Electronics and Applications, Singapore, May 2006, pp. 69–74

33 Calderón, A.J., Vinagre, B.M., and Feliu, V.: ‘Fractional order control strategies for power electronic buck converters’, *Signal Processing*, 2006, **86**, (10), pp. 2803–2819

34 Beltran, B., Ahmed-Ali, T., and Benbouzid, M.E.H.: ‘Sliding mode power control of variable-speed wind energy conversion systems’, *IEEE Trans. Energy Convers.*, 2008, **23**, (2), pp. 551–558

35 Wind Turbine Generator Systems, Part 21: Measurement and Assessment of Power Quality Characteristics of Grid Connected Wind Turbines, IEC Standard 61400-21

36 Baggini, A.: ‘Handbook of Power Quality’ (Wiley, 2008), pp. 525–526

37 IEEE Guide for Harmonic Control and Reactive Compensation of Static Power Converters, IEEE Standard 519-1992

Figure captions

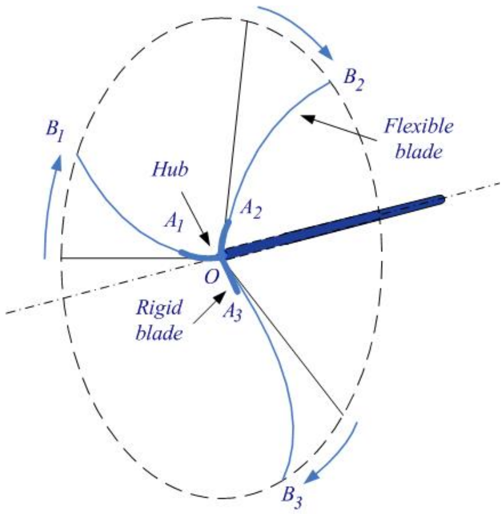

Fig. 1 *Blade bending dynamics for the three-mass drive train model*

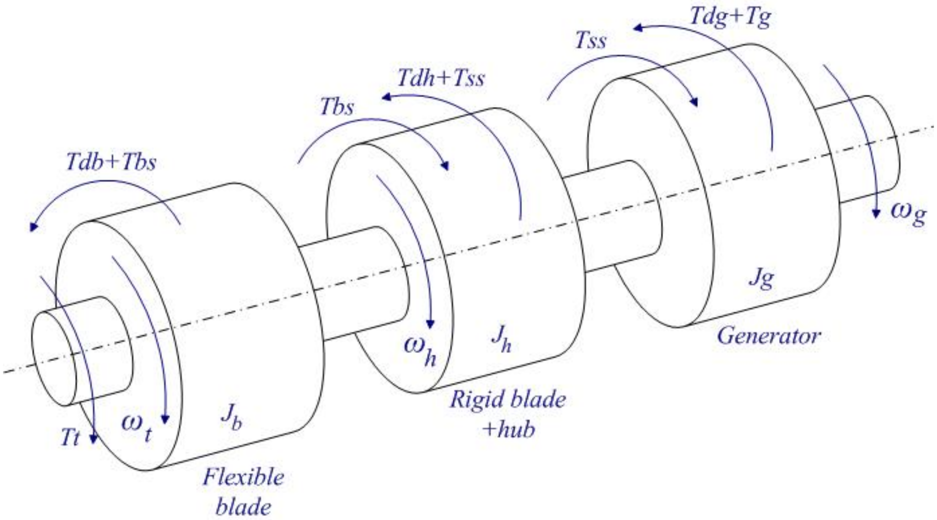

Fig. 2 *Configuration of the three-mass drive train model*

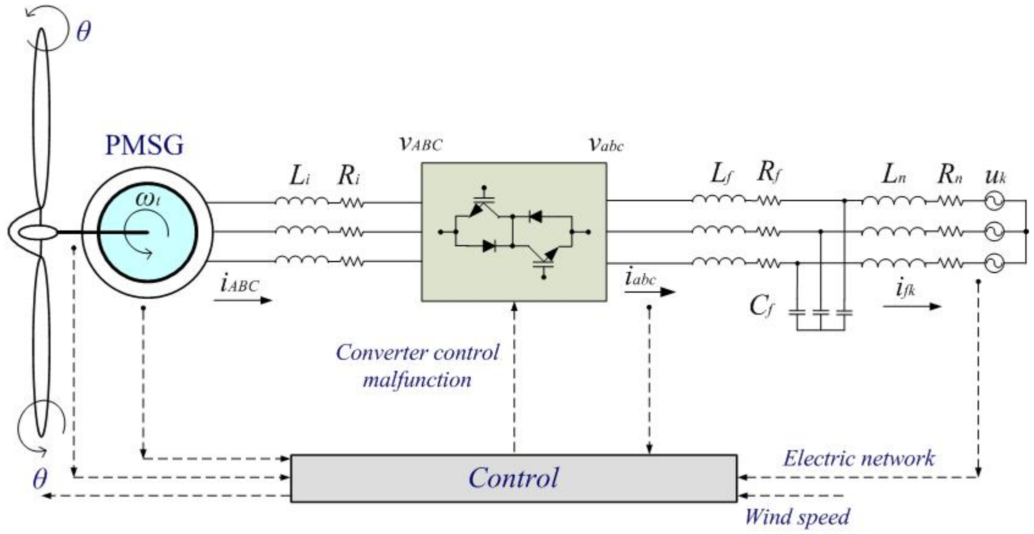

Fig. 3 *Wind power system with matrix converter*

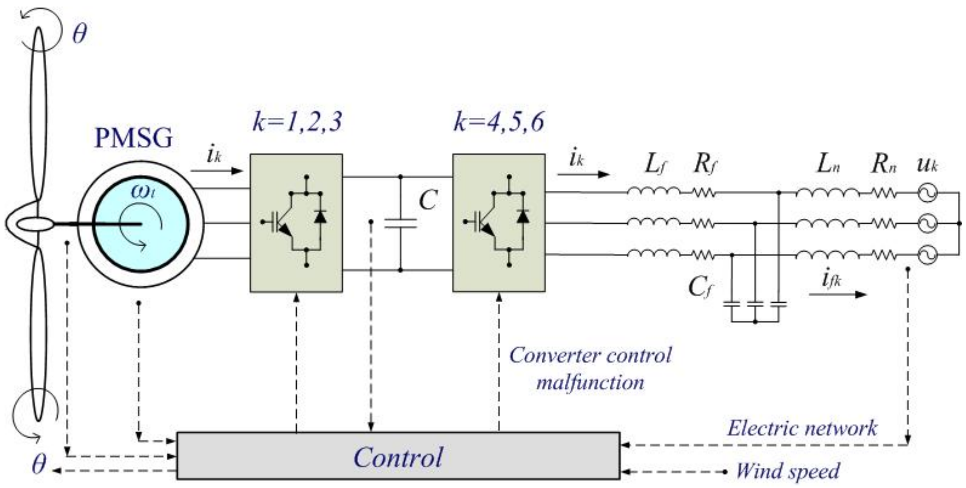

Fig. 4 *Wind power system with two-level converter*

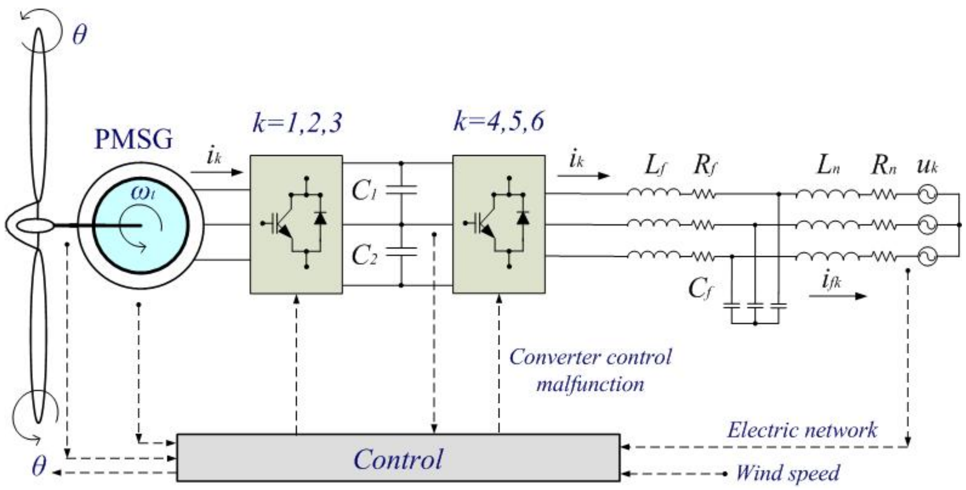

Fig. 5 *Wind power system with multilevel converter*

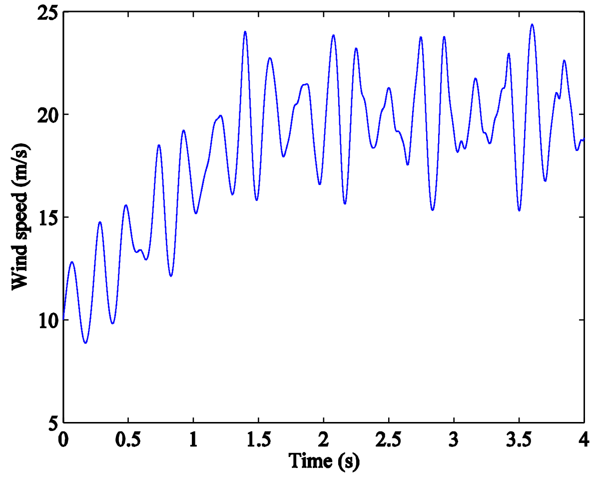

Fig. 6 *Wind speed profile*

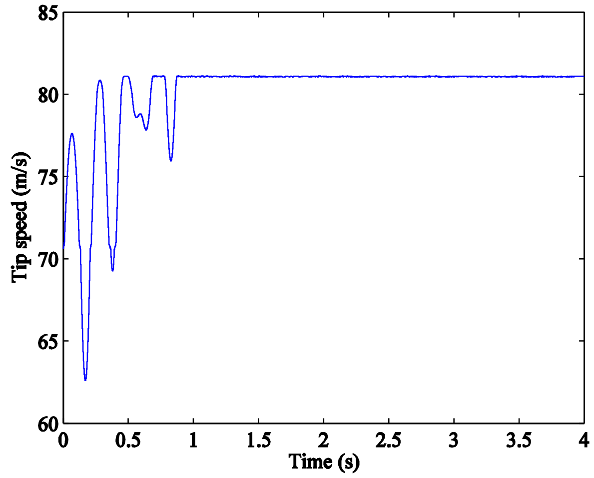

Fig. 7 *Tip speed of the blades*

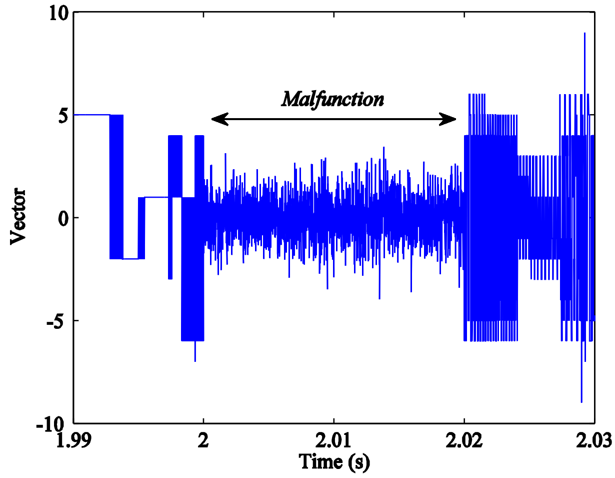

Fig. 8 *Vectors selection for the matrix converter and a three-mass model*

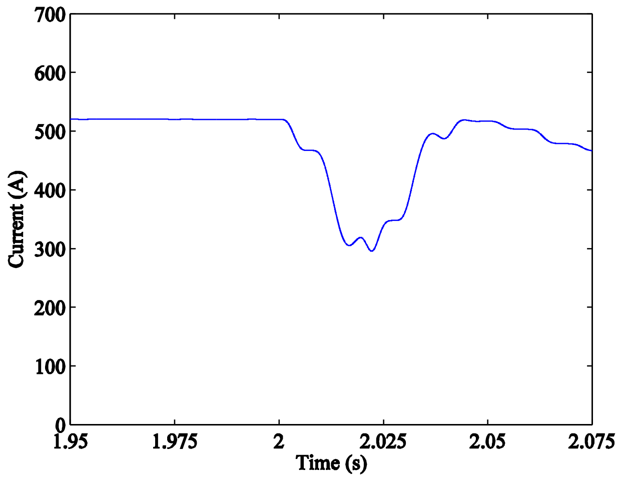

Fig. 9 *Output RMS current for the matrix converter and a three-mass model*

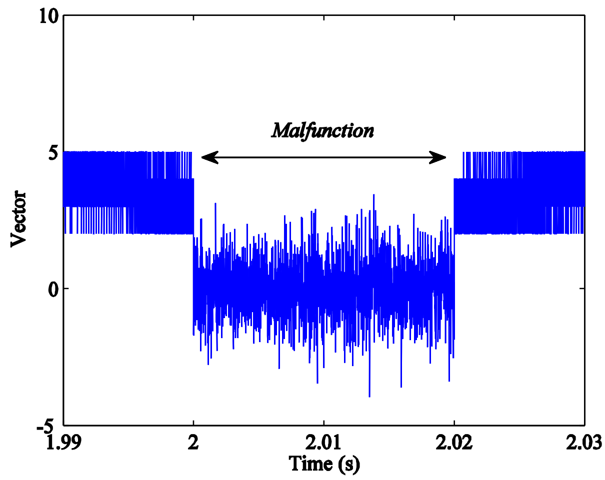

Fig. 10 *Vectors selection for the two-level converter and three-mass model*

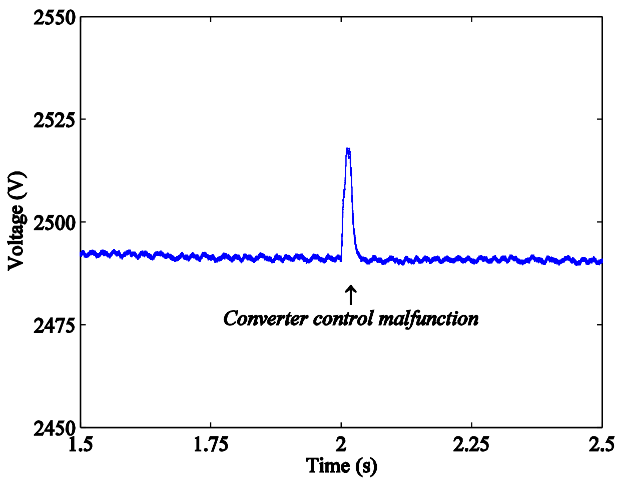

Fig. 11 *Voltage* v_{dc} *for the two-level converter and a three-mass model*

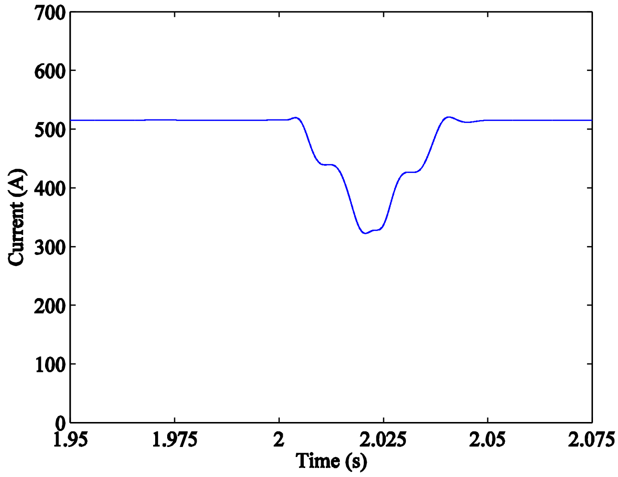

Fig. 12 *Output RMS current for the two-level converter and a three-mass model*

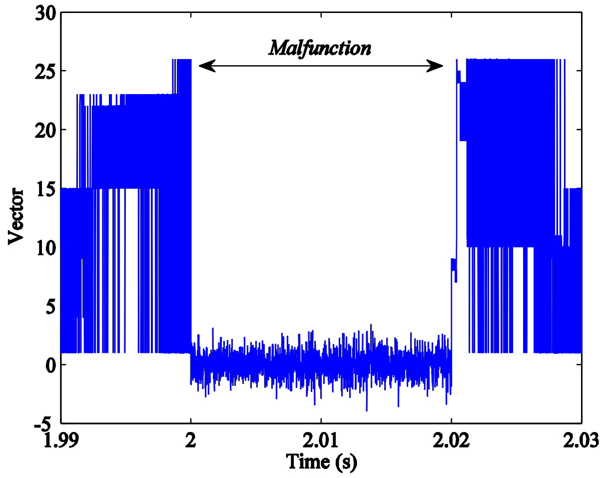

Fig. 13 *Vectors selection for the multilevel converter and three-mass model*

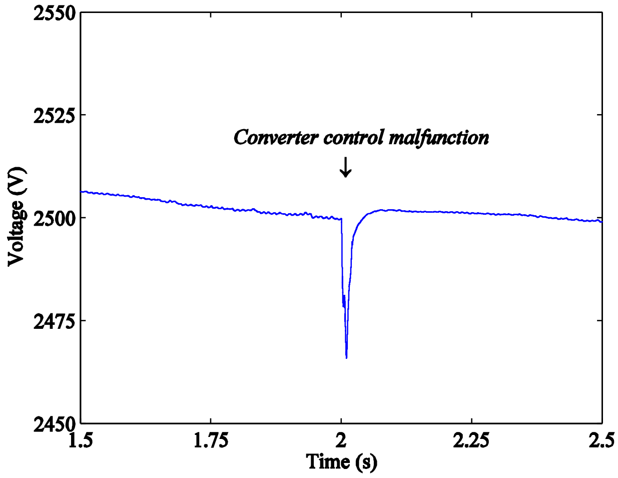

Fig. 14 *Voltage* v_{dc} *for the multilevel converter and a three-mass model*

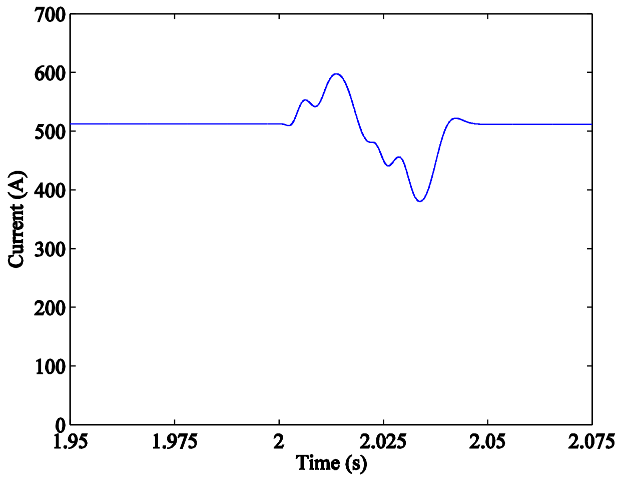

Fig. 15 *Output RMS current for the multilevel converter and a three-mass drive train model*

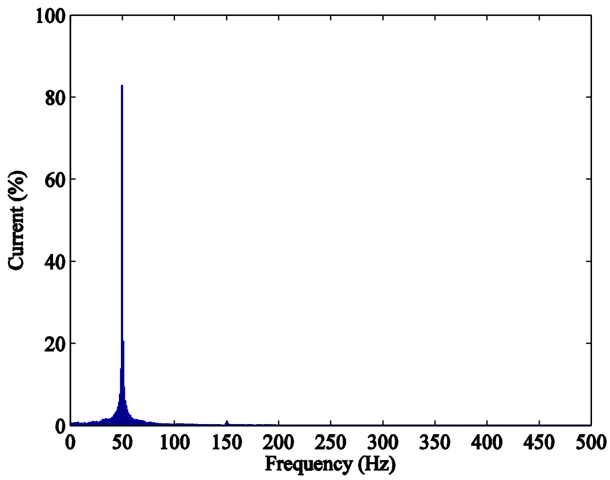

Fig. 16 *DFT of the current injected into the electrical grid for the matrix converter and a three-mass model*

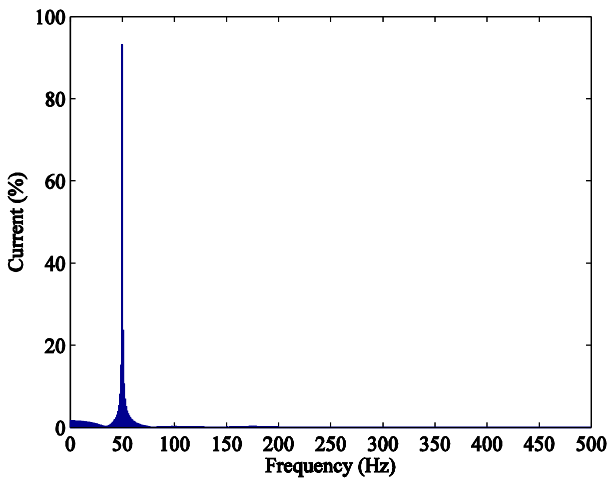

Fig. 17 *DFT of the current injected into the electrical grid for the two-level converter and a three-mass model*

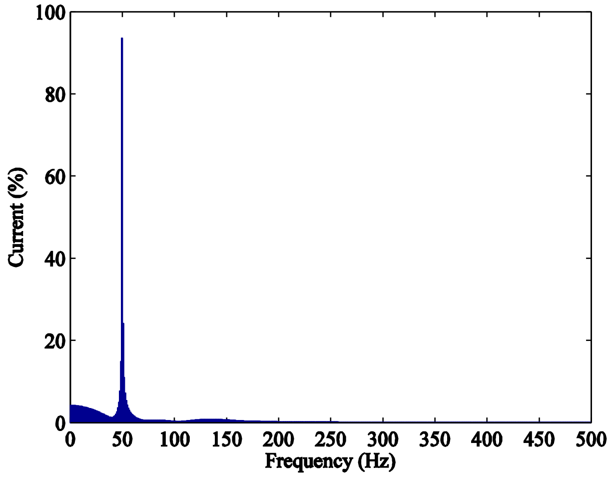

Fig. 18 *DFT of the current injected into the electrical grid for the multilevel converter and a three-mass model*

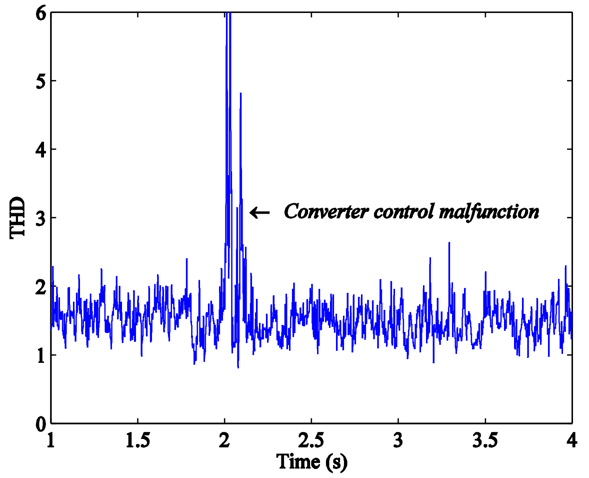

Fig. 19 *THD of the current injected into the electrical grid for the matrix converter and a three-mass model*

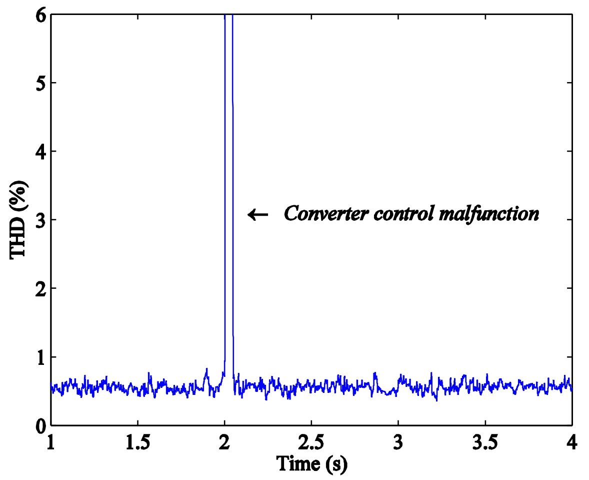

Fig. 20 *THD of the current injected into the electrical grid for the two-level converter and a three-mass model*

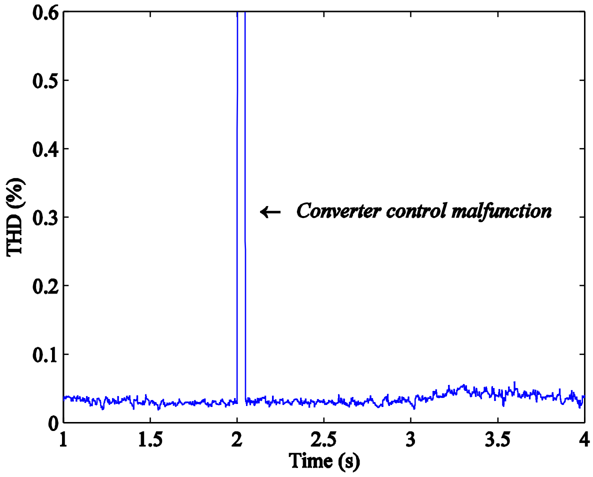

Fig. 21 *THD of the current injected into the electrical grid for the multilevel converter and a three-mass model*